An extreme precipitation event in Central Norway

By BIRTHE MARIE STEENSEN[1]*, HARALDUR ÓLAFSSON[1,2,3] and MARIUS O. JONASSEN[1],
[1]*Geophysical Institute, University of Bergen, P.O. Box 7803, NO-5020 Bergen, Norway;* [2]*Department of Physics, University of Iceland, Reykjavik, Iceland;* [3]*Icelandic Meteorological Office, Bustadavegi 9, IS-150 Reykjavik, Iceland*

ABSTRACT

At the end of January and beginning of February 2006, an extreme precipitation event occurred over Central Norway. The precipitation in addition to warm temperatures produced flooding and landslides that caused considerable damage to infrastructure. The event is explored with conventional data, data from remote sensing and numerical simulations. It is shown that there was very little quasi-geostrophic forcing during the event and that the extreme precipitation is locally generated by strong and persistent winds impinging the mountains. The mountains in the southwestern part of Norway, far away from the precipitation, contributed significantly to the extreme, by blocking, deflection and enhancement of the low-level flow. The warm and humid air masses involved are shown to originate in the subtropics. Assessment of forecasts with different lead times reveal a sensitivity to a baroclinic system to the east of Newfoundland upstream of the event in Central Norway.

1. Introduction

At the end of January and beginning of February 2006, Central Norway experienced an extreme precipitation event. The precipitation occurred together with high temperatures and snow melting that lead to severe flooding, damage to infrastructure and loss of human life. Several stations measured record high 24-h accumulated precipitation on 31 January 2006 UTC. The Norwegian Meteorological Institute did not however issue an extreme weather warning, as the customs are when high precipitation amounts combined with high temperatures are at risk of producing a large enough flood to cause damage. Although the seriousness of these kind of events and the importance of forecasting them accurately, they have not been described in detail in the scientific literature and the capability of the current state-of-the-art numerical models to reproduce such events needs to be explored.

A sole study, to the knowledge of the authors of this paper, describes an event of a similar kind over Western Norway, but with a primary emphasis on the large-scale circulation and the origin of the air masses transported from low latitudes with two extratropical cyclones that had undergone transition from two hurricanes. The high precipitation rates occurs when the warm air masses reaches the topography of Western Norway (Stohl et al., 2008). The flow pattern of air masses as it impinges

a mountain ridge depends on the non-dimensional mountain height $\hat{h}$, defined as $\hat{h} = \frac{hN}{U}$ (where U is the upstream horizontal wind speed, h is the mountain height and N is the Brunt-Väisälä frequency that describes the buoyancy on a vertically displaced air parcel). For low $\hat{h}$ the flow goes over the mountain, and the topography effect is significant. When the mountain height or the atmospheric stability increases, the mountain blocks the flow. The flow over the mountain will decrease, instead the flow on the sides of the mountain will increase (e.g. Pierrehumbert and Wyman, 1985; Ólafsson and Bougeault, 1996).

There are more studies of extreme precipitation in this region of the world in a climate change context. In a study of springtime precipitation and high temperatures, Benestad and Haugen (2007) conclude that high-rainfall–high-temperature events can become more frequent and produce a greater risk of spring time flooding in a future climate. In fact, downscaling of global climate simulations with regional climate models indicate higher rainfall intensity and warmer temperature in Western Norway in the future (Hanssen-Bauer et al., 2003; Beldring et al., 2008; Haugen and Iversen, 2008).

In this paper, the 2006 wintertime extreme precipitation event over Central Norway is studied. The meso- to synoptic-scale flow pattern associated with the event is described and the ability to reproduce the event by a Numerical Weather Prediction (NWP) model is evaluated with the help of measurements from a network of precipitation observations collected trough the Norwegian Meteorological Institute climate database (eklima.no) and satellite observations. Figure 1 shows where stations and other locations that are mentioned in the text are

---

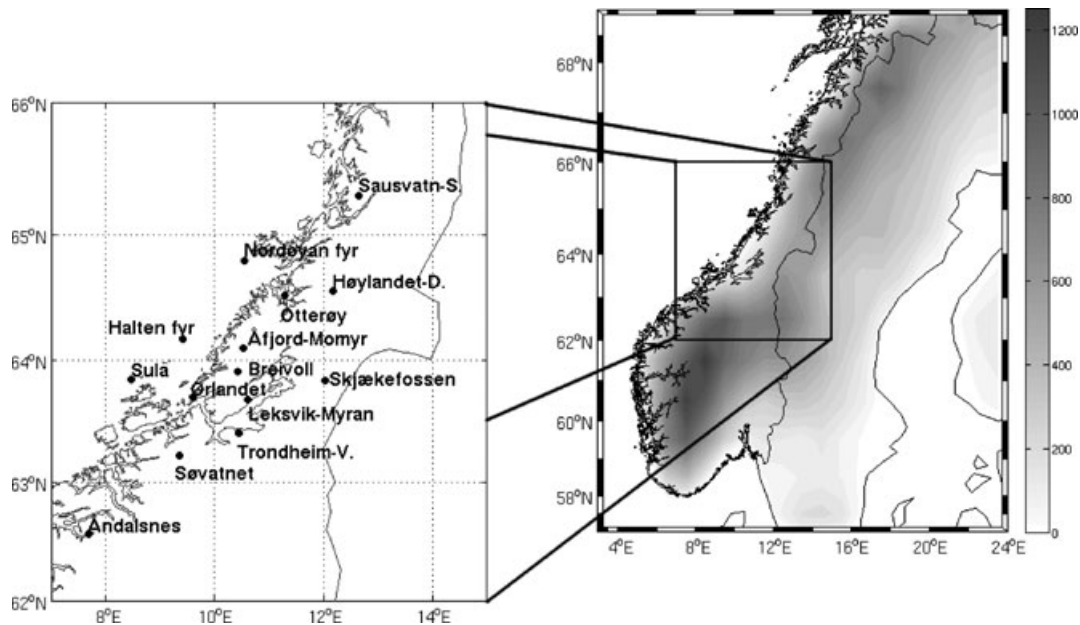*Corresponding author.
e-mail: birthesteensen@gmail.com

Fig. 1. Map of the different stations and areas mentioned in the text.

situated. The NWP tool is also used to establish the roles of synoptic-scale forcing and the topographic enhancement associated with the event. A trajectory model is used to trace back the origin of the air masses, and the predictability of the event is studied with the use of the numerical model and different initial times.

The second section of this paper gives a short description of the synoptic situation during the event; the third section is a short description of the model used for the simulations. The results are presented in the fourth section, followed by a discussion, summary and conclusions.

2. The synoptic situation

The synoptic situation during the event was characterized by a high-pressure over Great Britain with low-pressure systems to the west and east of it. Figure 2(a) shows the mean geopotential height at 500 hPa over 3 d from 29 to 31 January 2006. There is a distinguished omega shape pattern in the pressure field, which indicates a very stationary blocking event. The areas affected by a blocking event can experience the same kind of weather for an extended period of time as was the case during the event studied here. Figure 2(b) shows the anomaly of the geopotential height at 500 hPa over the same period, the geopotential height over Great Britain is more than 300 m higher than the average. The two lows, one south of Greenland and the other one over Russia are also shown. Figure 2(c) shows the temperature anomaly at 500 hPa. Over Central and Southern Norway, the temperature is 6-8 K above average. The maximum positive anomaly of 10 K

is located southeast of Iceland, while in Southern Europe the temperatures are lower than average.

Central Norway experiences heavy precipitation for several days. Figure 3(a) shows the observed accumulated precipitation for 5 d from 06 UTC 28 January to 06 UTC 02 February. The measurements are corrected for losses due to aerodynamical effects, adjusted for height differences between station point and grid point and interpolated to a 1-km grid, for more information see Mohr (2008). Figure 3(b) shows 24-h accumulated precipitation measurement series over the same 5 d from the four inland stations that had the highest measured precipitation in addition to measurement taken at the coastal Ørlandet station for observations taken at 06 UTC every day. The highest 24-h accumulated precipitation measured is from the observations at 06 UTC on 31 January. Åfjord-Momyr had the highest measured precipitation of all the stations with 143.9 mm per 24 h, this is the record high measured 24-h accumulated precipitation for this station, the next day it measured 113.5 mm per 24 h. The precipitation mean at Åfjord-Momyr station are 175 mm and 147 mm for January and February, respectively, this means that around 80% of the precipitation expected during the 2 months fell over 48 h. Several other stations also received record high precipitation measurements on 31 January 06 UTC: Otterøy measured 101.5 mm per 24 h while the January mean is 141 mm, and Halten fyr (lighthouse) measured 54.5 mm per 24 h and the January mean is 79 mm. All the stations in Fig. 3(b) are situated on the Fosen peninsula except for Otterøy, which is situated just north of it. This is in agreement with Fig. 3(a) that also shows most precipitation over the peninsula and in surrounding areas.
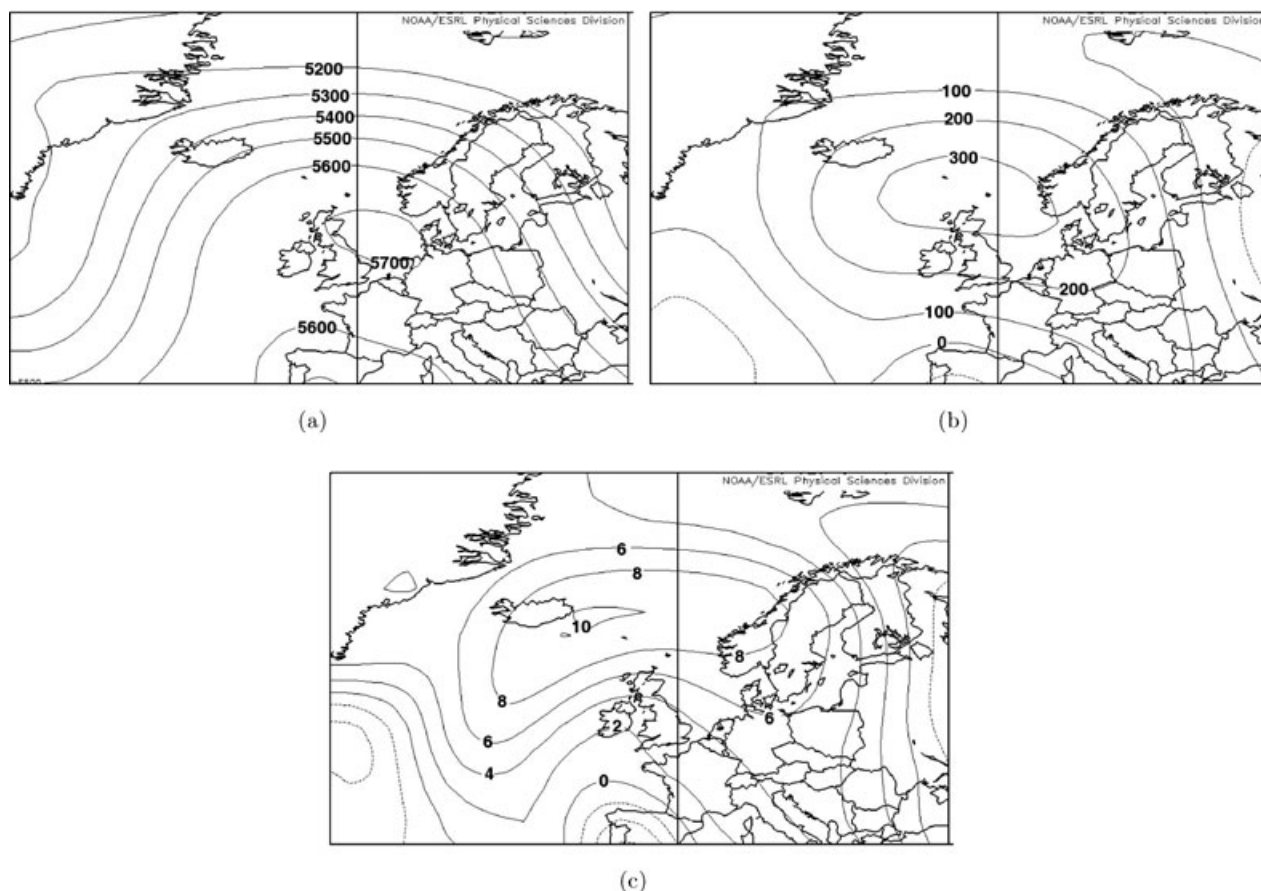
Fig. 2. Synoptic plots for 29–31 January 2006 (a) mean geopotential height (m) at 500 hPa with intervals of 50 m; (b) mean geopotential height anomaly from the Climatology mean (1968-1996) at 500 hPa with intervals of 50 m; (c) temperature anomaly at 500 hPa (intervals of 2 K). Data from NCEP/NCAR, acquired through NOAA/CDC (Kalnay et al., 1996).
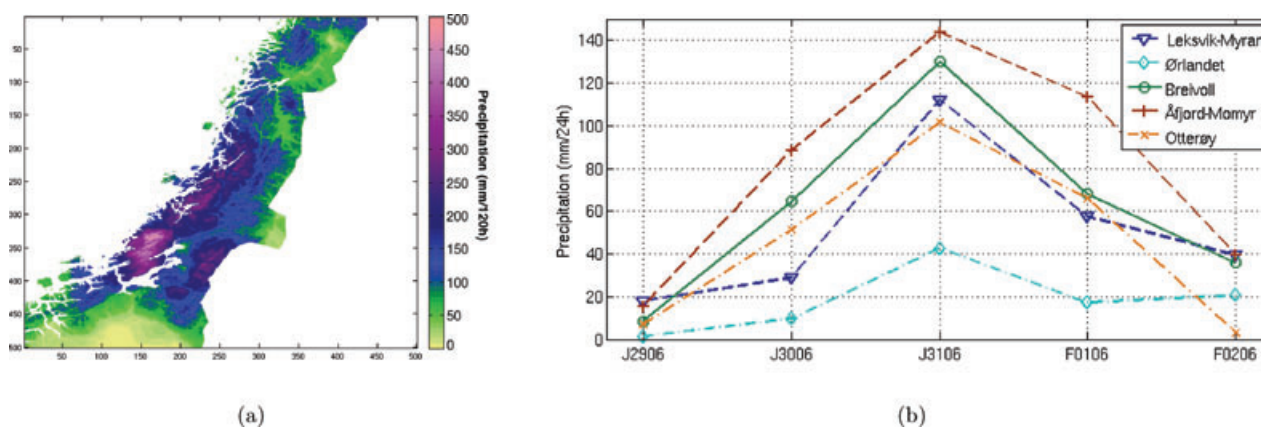

Fig. 3. (a) Interpolated measured 120 h accumulated precipitation with 1 km resolution (Mohr, 2008) from 06 UTC 28 January to 06 UTC 2 February. (b) Accumulated precipitation (mm per 24 h) measured at 06 UTC from five stations from 29 January to 2 February.

3. The numerical simulations

The period was simulated using the Weather Research and Forecasting (WRF) Model, version 3.0.1. The Advanced Research WRF (ARW) solver integrates the compressible, non-hydrostatic Euler equations. For more details on the model see Skamarock et al. (2008). Pre-processing programs set up the grids and interpolates European Centre for Medium-Range
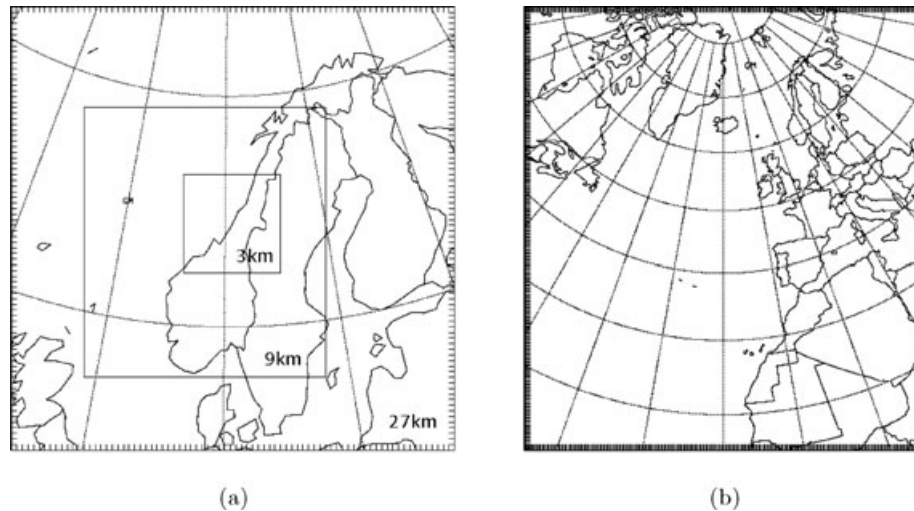
Fig. 4. (a) The 27, 9 and the 3 km domain, and (b) the large domain with 27 km resolution for the predictability study.

Weather Forecasts (ECMWF) data to use as initial conditions, as well as to generate lateral boundary conditions. The ECMWF data have a 0.5° horizontal resolution and a temporal resolution of 6 h.

The model was run with a horizontal grid cell resolution of 27, 9 and 3 km (see Fig. 4a for domain locations). All the simulations were run with 29 vertical levels and with one-way nested domains. The control simulation (CTRL) starts at 00 UTC 29 January and runs for 120 h until 00 UTC on 3 February. In addition, two sensitivity tests are simulated over the same time period, but with different parts of the topography removed. In the first sensitivity test, all the topography south of Lofoten is removed, this run will be referred to as NOTOPO BIG. In the second, only the mountains in the southern part of Norway are removed. This mountain ridge is called Langfjella, so this sensitivity test will be referred to as NOTOPO LANG. Figure 5 shows the different topography for the different runs in the 27 km domain.

To test the predictability of this event, several simulations with different initialization times are carried out. Figure 4(b)

shows the domain for these simulations, only a coarse domain of 27 km resolution is used and the domain includes a large part of the North Atlantic, East Canada, Europe and Northwest Africa. The longest simulation of this kind starts at 00 UTC on 25 January, there is one new simulation started every 24 h until the 29 January. All these simulations end at 00 UTC 3 February.

4. Results

4.1. Validation

To validate the simulation of the event, precipitation measurements from weather stations taken at 06 UTC 31 January are compared with 24-h accumulated precipitation over the same time period from the 3 km and 9 km domain in the CTRL simulation. Figure 6 shows the measured precipitation from 14 rain gauges, and modelled precipitation interpolated from the nearest grid points to the same 14 stations. Overall, the simulation agrees quite well with the observations, except at Søvatnet and at the four stations with the highest measured
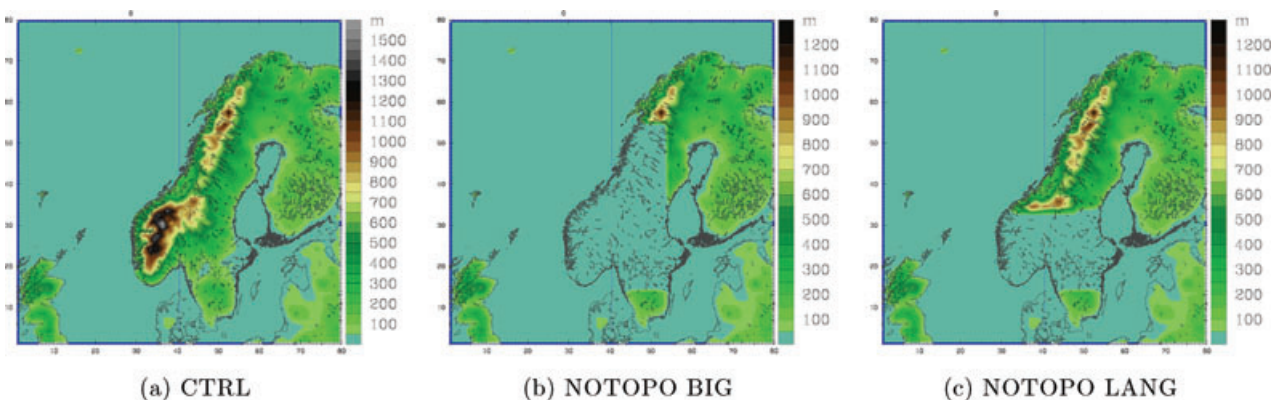

Fig. 5. Topography in the three different simulations. (a) CTRL, (b) NOTOPO BIG and (c) NOTOPO LANG.
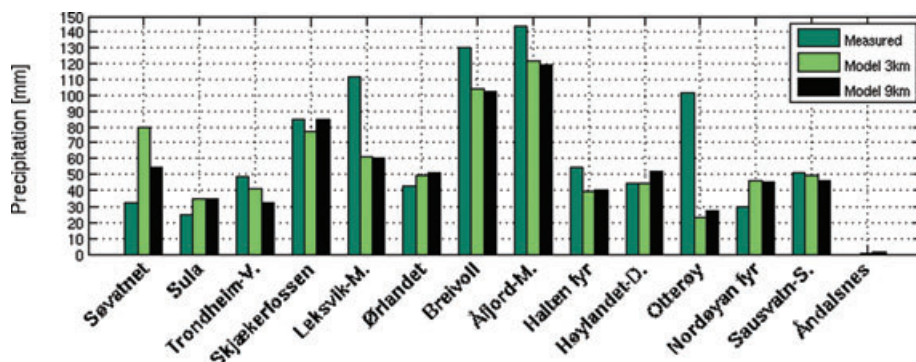
Fig. 6. Measured and modelled 24-h accumulated precipitation from the 3 km and 9 km domain for 14 different stations.

precipitation. At Søvatnet, which is located 306 m above sea level south of the extreme precipitation area, the model produces almost two and a half times the measured precipitation in the 3 km domain. On the other hand, the model underestimates the precipitation at the four stations with the highest measured precipitation. Leksvik-Myran, Breivoll and Åfjord-Momyr are all situated on the Fosen Peninsula. The model produces 55% of the measured precipitation at Leksvik-Myran, which is located on the lee-side of the peninsula. The precipitation at Otterøy which is located just north of the peninsula, 36 m above sea level, the model only produces 23% of the precipitation in the 3 km domain and 27% in the 9 km domain. This makes Otterøy the worst represented station by the model of all the stations used in this study.

Figure 7 shows the measured and modelled 24-h accumulated precipitation field over Trøndelag. The observed and gridded precipitation field is located more to the south than in the model, this corresponds to the overestimation at Søvatnet. However the fields where there is maximum precipitation correspond quite well.

Radar images are not available, but over the ocean, satellite observations of precipitation can be used to compare with the simulation (Fig. 8a). The satellite data are from the Hamburg

Ocean Atmosphere Parameter (HOAPS) archive, it contains 1° twice daily multisatellite composite products (Andersson et al., 2007). The precipitation data are derived by passive microwave radiometers from the Special Sensor Microwave/Imager (SSM/I) (Wentz and Spencer, 2008). The grid cells contain a composite of data from satellites that passed the grid box closest to 12 UTC and 24 UTC. Figure 8 shows satellite precipitation data for the 12 UTC passes 30 January and 3 h accumulated precipitation 12 UTC 30 January from the 9 km domain CTRL run. Both the satellite precipitation data and the modelled precipitation show very low precipitation rates over the ocean compared to the rates over land. In spite of some differences, the overall quality of the simulation must be characterized as quite good.

4.2. The synoptic scale forcing

According to classic quasi-geostrophic theory, the large-scale ascending motion needed for precipitation is related to either differential advection of vorticity or advection of temperature. During wintertime most cases of heavy precipitation is associated with fronts and upper level troughs (Holton, 2004). Figures 9(a) and (b) show vorticity and the geopotential at 300 hPa, and temperature and wind at 850 hPa, respectively. The
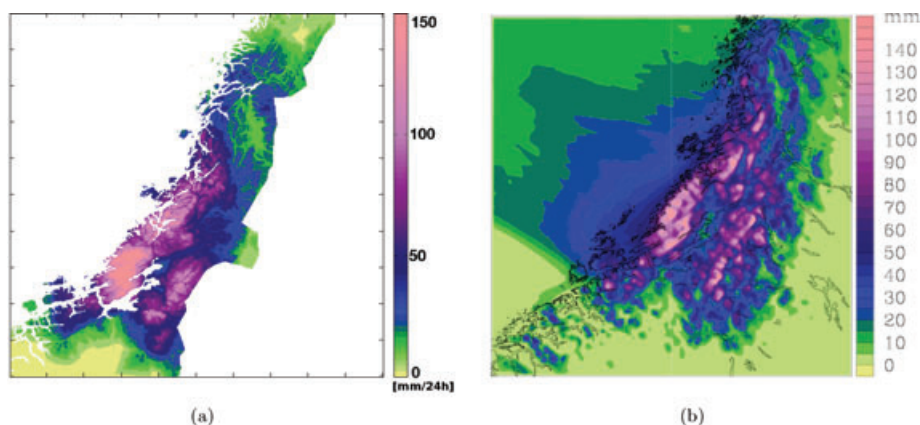

Fig. 7. (a) Interpolated measured 24-h accumulated precipitation with 1 km resolution (Mohr, 2008) from 06 UTC 31 January 2006, (b) modelled 24-h accumulated precipitation in the 3 km domain CTRL run for the same time.
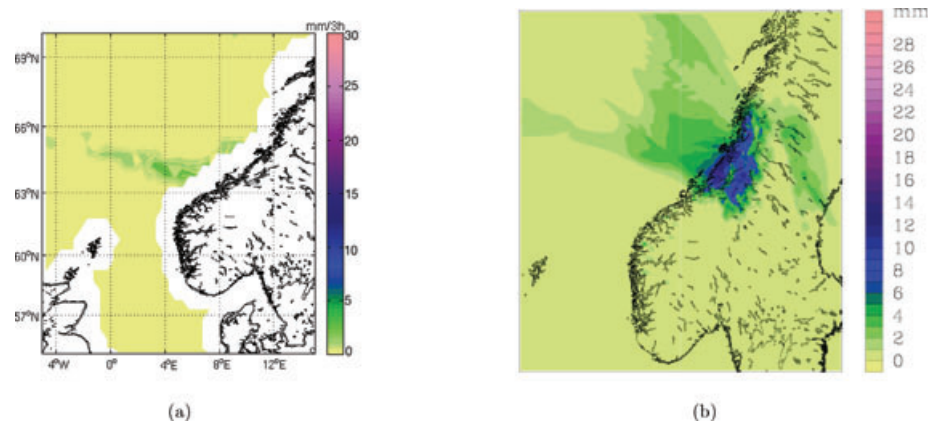
Fig. 8. (a) Satellite precipitation data (mm per 3 h) over Northern Europe for 30 January 12 UTC passes from the HOAPS archive, (b) simulated precipitation (mm per 3 h) at 12 UTC 30 January from the 9 km domain.
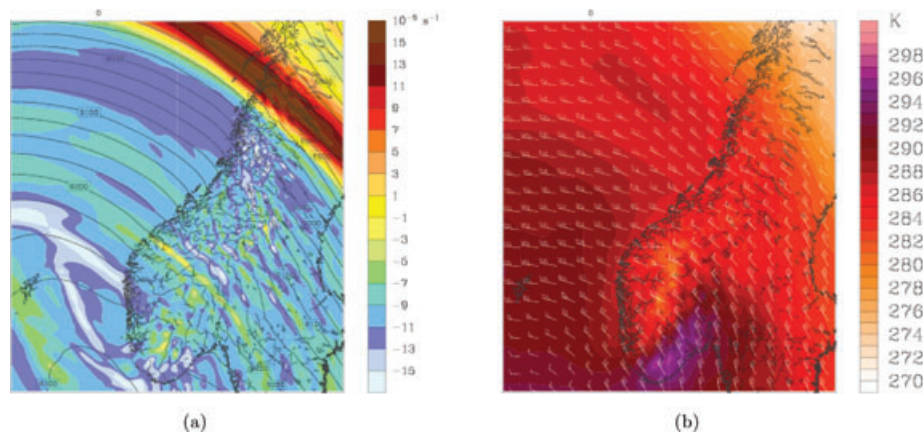

Fig. 9. (a) Vorticity and geopotential height at 300 hPa with a 25 m interval, (b) potential temperature and wind vectors at 850 hPa, both at 18 UTC on 30 January in the 9 km domain.

figures reveal that there is no advection of vorticity at higher levels and limited temperature advection at lower. The large-scale forcing for ascending motion and precipitation described by the omega equation was in other words of very limited magnitude during this event.

4.3. Sensitivity to topography

There is a large difference in the accumulated precipitation between land and ocean during the event and the orographic enhancement plays an important role in extreme precipitation in Norway. Removing different parts of the topography can help to highlight these effects. As mentioned, two different simulations were done without topography.

Table 1 shows 3-h accumulated precipitation at 12 UTC 30 January for six stations in the 3 km domain, see Fig. 1 for the location of these stations.

There is a clear influence of topography. The simulation where most Scandinavia's topography is removed (NOTOPO BIG), produced about one third of the precipitation in the CTRL

simulation, and the precipitation rates have less variation between the different stations. For the coastal station (Ørlandet), the NOTOPO LANG simulation produces more precipitation than the CTRL run. Yet for the other stations the precipitation rates amount to only 21–60% from the CTRL simulation. The different precipitation pattern between the CTRL and NOTOPO LANG simulation that Table 1 presents, illustrates the significance of the topography in Southern Norway affecting the flow pattern over Central Norway (Trøndelag).

Figures 10(a)–(c) show the wind pattern in the 9 km domain at 925 hPa on 30 January 12 UTC for the different topography simulations, and (d) and (e) show the difference between the CTRL and the other topography simulations. The CTRL simulation has the greatest wind speed over Central Norway, about 8 m s^{-1} more than the NOTOPO LANG and NOTOPO BIG simulations. The wind direction in the CTRL run is more westerly than for the two other simulations. Both the NOTOPO simulations give much stronger winds than the CTRL simulation at the west coast of Norway, south of our area of interest. It is evident that the Langfjella mountain ridge acts as a blocking for the prevailing

Table 1. 3-h accumulated precipitation for 30 January 12 UTC for the three different topography simulations from the 3 km domain.

Model	Ørlandet	Breivoll	Åfjord-M.	Trondheim-V.	Skjækefossen	Høylandet-D.	Average
CTRL	4.5	10.5	14.4	4.0	10.2	5.8	7.8
	100%	*100%*	*100%*	*100%*	*100%*	*100%*	*100%*
NOTOPO	5.6	8.0	9.0	3.2	7.0	3.2	5.7
LANG	*124.6*	*76.0%*	*62.7%*	*80.4%*	*69.0%*	*55.0%*	*73.1%*
NOTOPO	3.1	4.0	4.1	2.3	2.2	1.8	2.9
BIG	*69.0%*	*38.3%*	*28.3%*	*59.6%*	*21.3%*	*31.4%*	*37.2%*

(a) CTRL (b) NOTOPO LANG (c) NOTOPO BIG

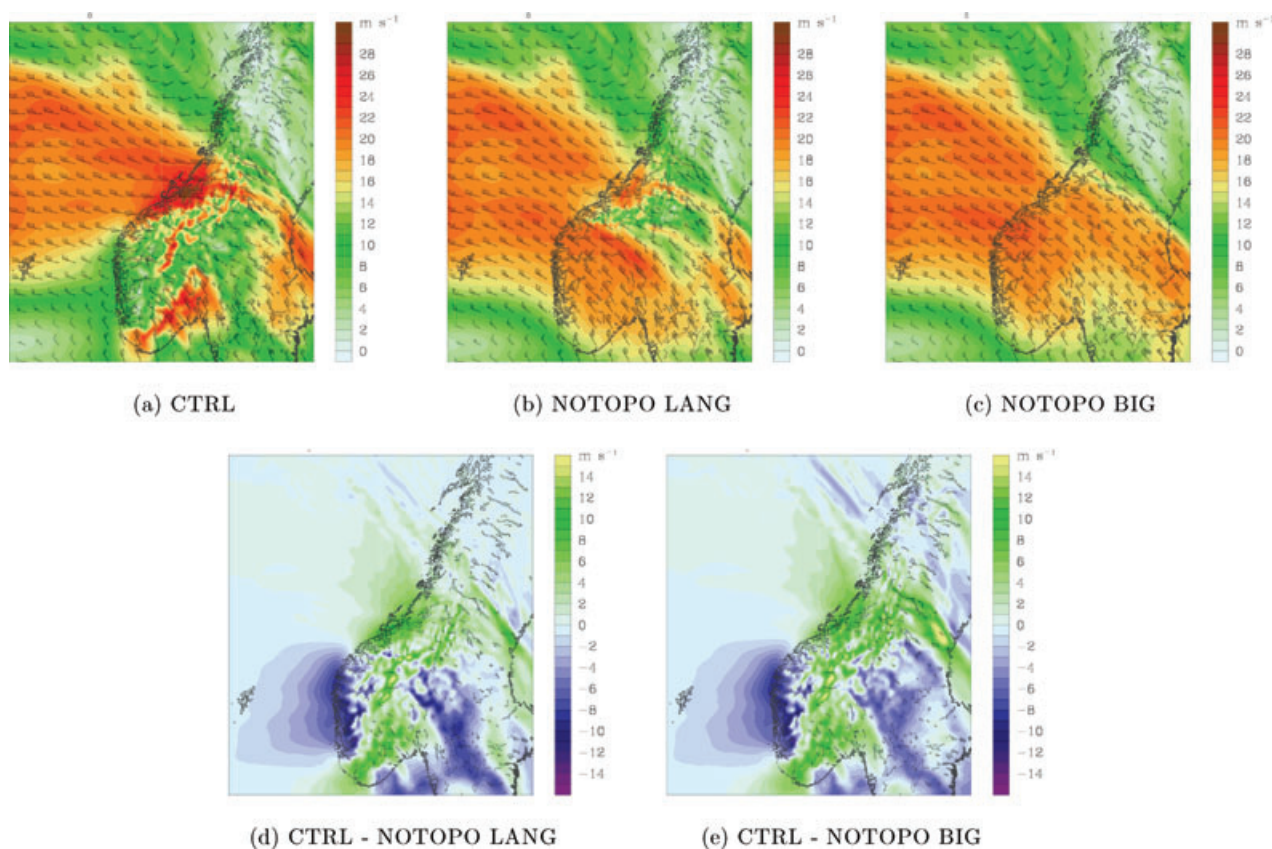(d) CTRL - NOTOPO LANG (e) CTRL - NOTOPO BIG

Fig. 10. (a–c) Winds at 925 hPa in the 9 km domain on 30 January at 12 UTC for the CTRL, NOTOPO LANG and NOTOPO BIG; (d) difference in wind speed between CTRL and NOTOPO LANG and (e) the CTRL and NOTOPO BIG difference.

west-northwest flow over Southern Norway and increases the wind speed in Central Norway.

4.4. The origin of the air masses

Trajectories are calculated by the HYSPLIT trajectory model using Reanalysis data from NOAA (Draxler and Rolph, 2010; Rolph, 2010). Figure 3(b) shows that the highest measured precipitation rates were between 06 UTC 29 January and 06 UTC 1 February. Trajectories are calculated backwards from a stopping altitude of 3500 m in (a) and 5000 m in (b) in the lower

part of the troposphere where most of the water vapour in the atmospheric rivers are contained. The trajectories are calculated over 120 h with 6-h intervals between each trajectory during this time period. Figures 11(a) and (b) show 13 trajectories for air parcels ending over the Fosen peninsula (lat:63,7/lon:9,6). All the trajectories at both stopping altitudes have a route between the British Isles and Iceland before the air parcels reach the coast of Central Norway. The trajectories in (a) from the beginning and the end of the period originate at around 40° N, and one is caught in the anticyclone over the British Isles. However the majority of these trajectories and all of the trajectories (b) which are
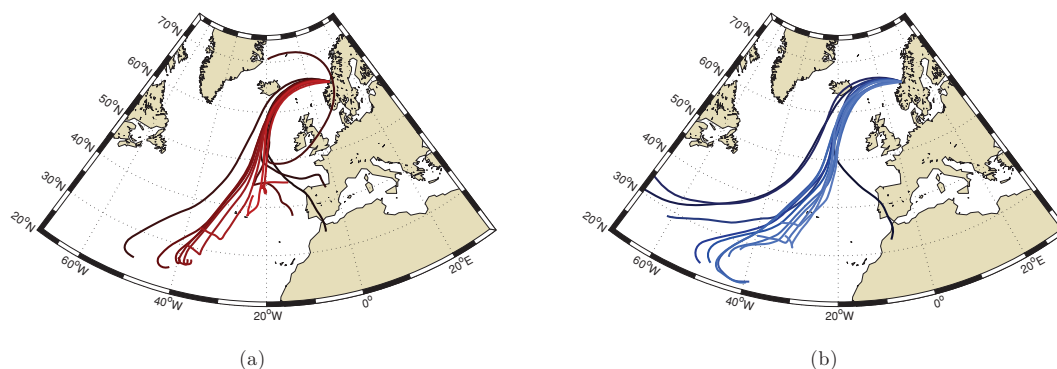
(a)   (b)

Fig. 11. Trajectories for different air parcels starting at 06 UTC on 29 January and ending over the Fosen peninsula at 06 UTC on 1 February with 6 h interval. The darkest trajectories are from the beginning of the period and they become lighter towards the end. (a) Parcels stopping 3500 m above the peninsula and (b) 5000 m above.

at higher altitudes, originate at subtropical latitudes. The warm moist air parcels that follow these trajectories travel over 40° of latitude northwards before ending up over the Fosen peninsula.

4.5. Sensitivity to initial conditions

To assess the forecast quality as a function of lead time, five simulations with different initial time are run over a large domain with 27 km grid size. Figure 12 shows the precipitation produced by the model with the different initial times onshore (a), and offshore (b). There is an almost linear decrease with increased lead time in the forecasted precipitation over land between the four simulations (except the latest initial time), while over the ocean this is not evident, and the simulation with latest initial time produces less than the simulations with initial time 24 and 48 h later.

Comparing the two simulations, initialized at 00 UTC on 28 January and at 00 UTC on 29 January, it is clear that both simulations produce little precipitation over the ocean, while the one initialized later (shorter lead time) does better in reproducing the enhancement of the precipitation over land. In the following, we
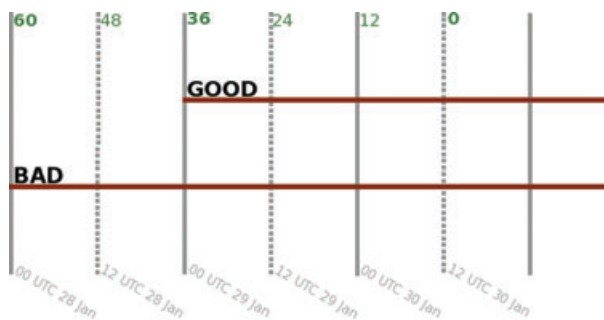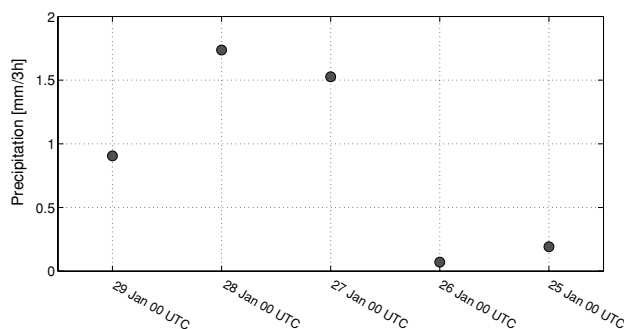

Fig. 13. Timeline of the GOOD and BAD simulations. The numbers above are hours before 12 UTC 30 January.

shall concentrate on the difference between these two simulations, in order to shed light on why the forecast with the longer lead time did worse in reproducing precipitation over land. In the following the simulation initialized at 00 UTC on 28 January will be referred to as BAD, while the simulation initialized at 00 UTC on 29 January will be referred to as GOOD. Figure 13 shows the time series of the GOOD and BAD simulations.
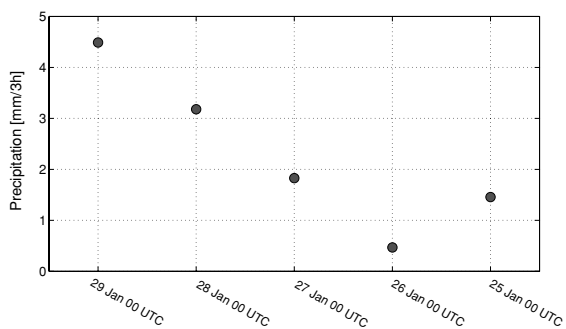
(a) Precipitation over land mm/3h   (b) Precipitation over ocean mm/3h

Fig. 12. Precipitation (mm per 3 h) produced by the model, as a mean over the time period from 9 UTC to 18 UTC 30 January, for the different lead times for the big 27 km domain. (a) Over land as a mean for nine different stations and (b) over the ocean as a mean for nine different points.
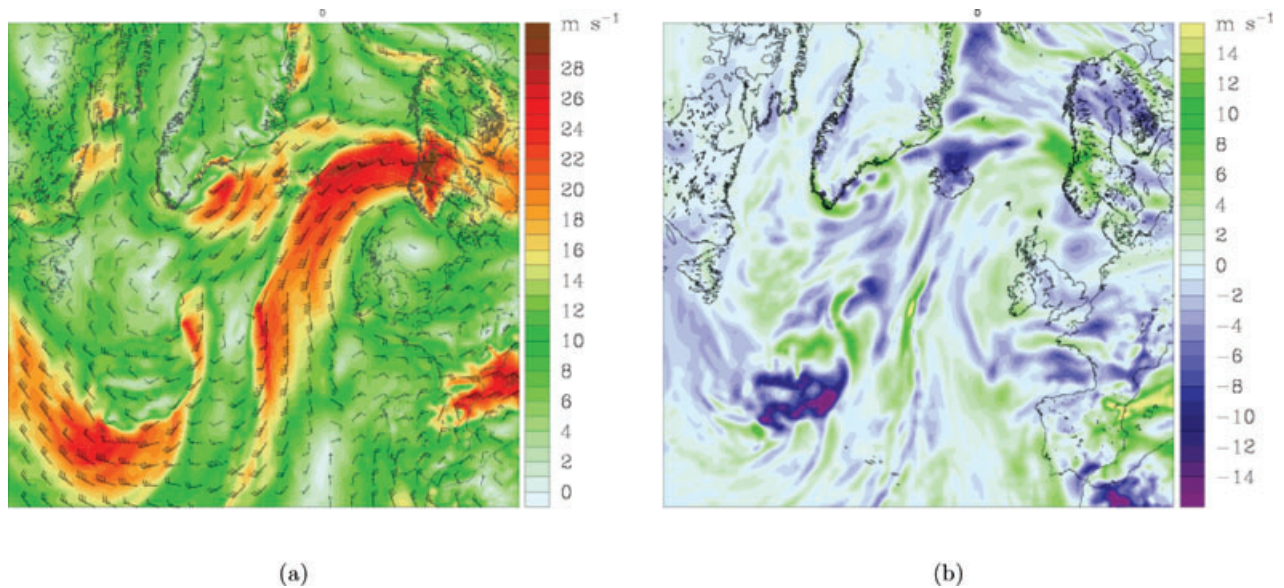
(a)   (b)

Fig. 14. (a) Wind field at 850 hPa at 12 UTC on 30 January in the GOOD simulation, and (b) the difference wind field (GOOD-BAD) at the same time.

Figure 14 shows the wind field at 850 hPa in the GOOD simulation (a) and the difference between the GOOD and the BAD simulation (b), both at 12 UTC on 30 January. In Central-Norway, the winds are strong and in the GOOD simulation they are about 8 m s^{-1} stronger than in the BAD simulation.

The low-level winds are close to geostrophic and in order to explore the origin of the difference in the wind fields, it is convenient to trace the differences between these two simulations in the surface pressure field (Fig. 15).

At the initial time for the GOOD simulation, this simulation has lower pressure between Greenland and Iceland (Fig. 15a). The circle shows how this difference in MSLP moves east, and at 12 UTC on 30 January the pressure difference is located over Trøndelag.

The lower pressure in the GOOD simulation is associated with higher low-level temperatures than in the BAD simulation. Figure 16(a) shows the differential temperature field between the GOOD and the BAD forecast at 850 hPa at 00 UTC on 29 January, and trajectories starting 24 h earlier and ending inside the temperature anomaly at 850 hPa on 00 UTC 29 January. Figure 16(b) shows the potential temperatures at 850 hPa with MSLP, a low pressure with a cold front is situated east of Newfoundland. Both trajectories trace directly backwards to the region of the cold front, suggesting very strongly that the temperature where the GOOD and the BAD simulations differ from each other is sensitive to the baroclinic development south of Greenland.

5. Discussion

Perhaps the most interesting result of this study is how the topography of Southern Norway (Langfjella) contributes to the precipitation in regions far north of these mountains. The non-dimensional mountain height for the Langfjella mountain ridge is too high for the impinging air flow to go over, and due to the Coriolis force, the large-scale flow symmetry around the mountain ridge is broken, and an increase of the flow occurs on the left from downstream (in the Northern Hemisphere, Ólafsson and Bougeault (1997)). The enhanced flow, in this case on the northern side of the Langfjella range, causes increased upslope forcing, which leads to enhanced precipitation in the impinging warm and moist air mass. Increased vertical velocities and precipitation on this side of a mountain range are also explored in Ólafsson (2000) and Hunt et al. (2001). However, in these two studies, the increased lifting was due only to asymmetry in the flow field and not direct lifting by the increased wind impinging the Central Norway mountains, as in this case. Ólafsson and Bougeault (1996) discovered that increased wind speed at the edge of a mountain range contributed to enhanced breaking of gravity waves on the flanks of the mountain, and called it secondary wave breaking. In line with this, we call the topographic effect from Langfjella a secondary topographic forcing of precipitation generation. The primary effect is the direct lifting of the air masses over the mountains in Central Norway.

It is also of interest that a lot of the precipitation is probably generated locally, by the strong flow impinging the mountains. This is in contrast to most large-scale precipitation systems in mid-latitudes, where fronts and upper level vorticity advection are the major factors (Holton, 2004). This case is an example of a case that is different from many other extreme precipitation cases in terms of atmospheric dynamics for Norway, where frontal precipitation is most common. A result of this kind should be
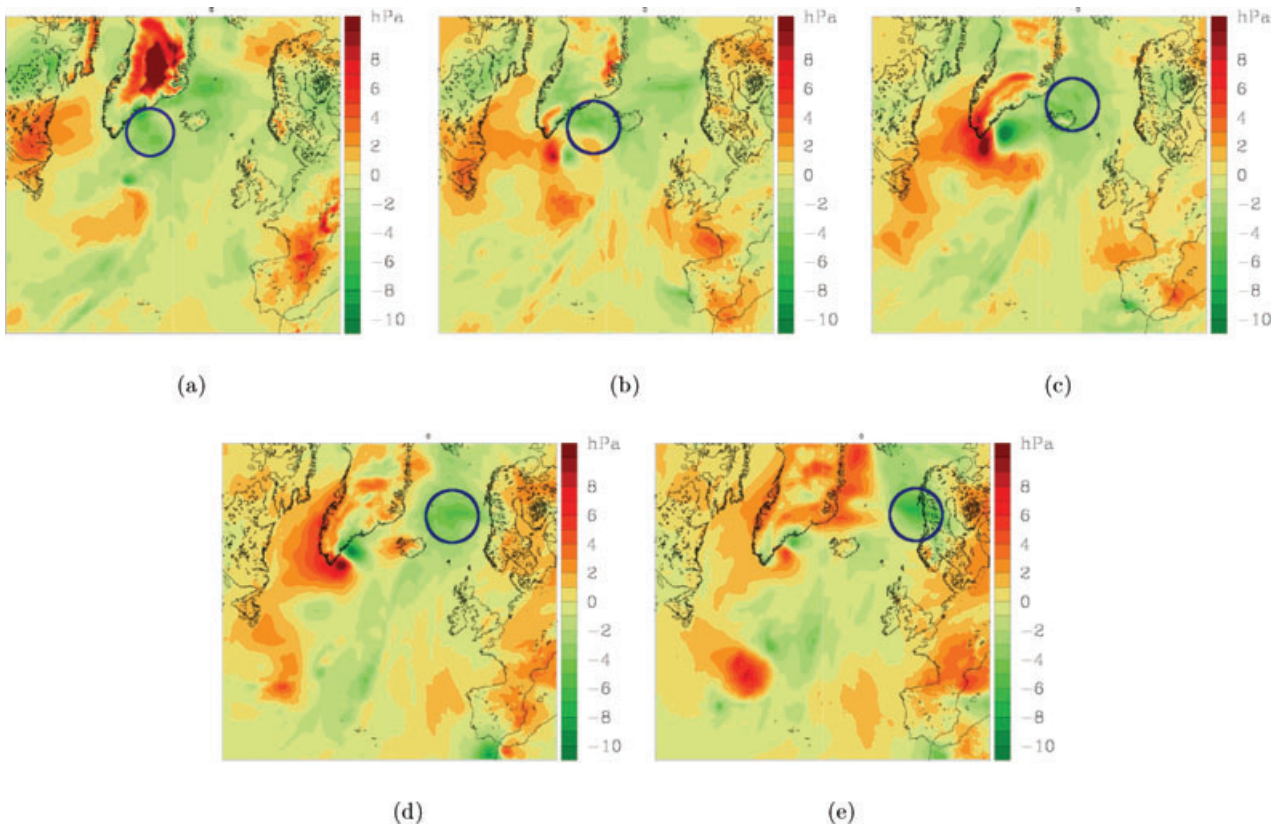
Fig. 15. The difference MSLP between the GOOD and the BAD simulations (GOOD–BAD) with 9 h intervals (a) 00 UTC 29 January, (b) 09 UTC 29 January, (c) 18 UTC 30 January, (d) 03 UTC 30 January and (e) 12 UTC 30 January. The circle shows the depression.
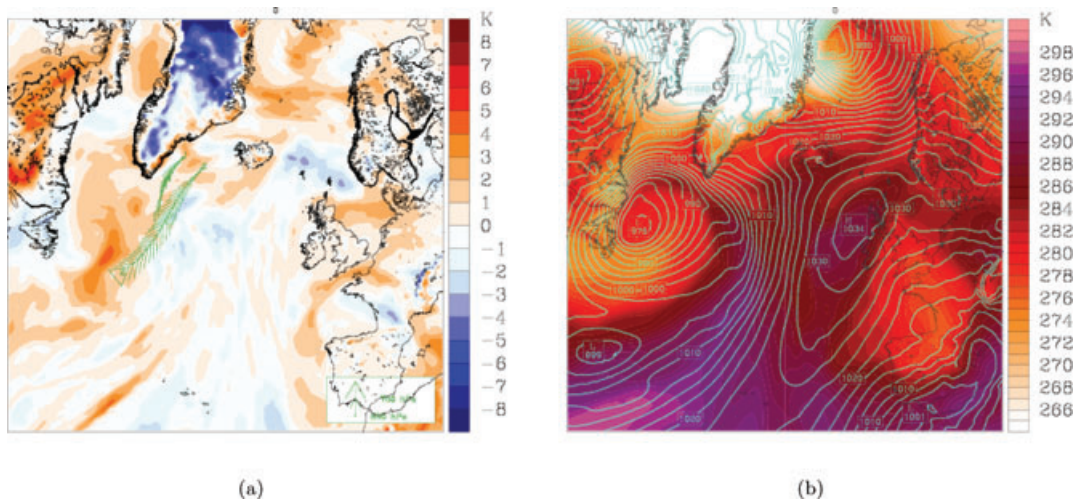

Fig. 16. (a) Difference field between GOOD and BAD (GOOD–BAD) potential temperature at 850 hPa at 00 UTC on 29 January and trajectories from 00 UTC on 28 January to 00 UTC 29 January. (b) Potential temperature in 850 hPa and MSLP with 2.5 hPa interval 00 UTC 28 January.

considered when statistically modelling the distribution of events of allegedly the same kind.

As in the study of Stohl et al. (2008), the air masses originate from the subtropics. Though during that event the transport was associated with two tropical hurricanes that underwent transition to extratropical cyclones. Occurring as late as at the end of January, no hurricanes were present in this event. A main point of interest in this context may be that in spite of the precipitation

being generated by perturbations on mesoscale, a certain large-scale quasi-stationary flow pattern is needed.

The large spatial variability in the precipitation in the present case is not surprising and must be related to variability in the small-scale forcing as described for instance in Reuder et al. (2007) for flow over complex topography in Western Norway.

In this paper, we present quite a novel approach to assessing what goes wrong in a forecast. A similar approach has been introduced in the theses of Hagen (2008) and Tveita (2008). Drawing very conclusive conclusions from tracing back air masses in a region where a new analysis gives a field that is different from a 24 h forecast can of course be questioned. The result, leading us to an upstream baroclinic zone is however in agreement with a common result of sensitivity area predictions pointing at areas in the baroclinic zone below the jet, upstream of the verification areas, indicating that improved observations in these zones may lead to better forecasts downstream (e.g. Rabier et al., 1996).

A final point of interest is the fact that during this winter season, the NAO index was negative. In such conditions, mean precipitation should be expected to be less than average in Central Norway. Yet, the present case has extreme precipitation. This underlines the fact that individual extreme events, even though they may last for several days do not necessarily follow mean seasonal values.

6. Summary and conclusions

The main conclusions of this study is that the extreme precipitation event during winter 2006 in Central Norway was to a large extent generated by local topographic forcing, even though the precipitation extended over a large area and the air masses originated in the subtropics. The dominating topographic effect was direct lifting of the impinging air masses, while a secondary topographic effect was the enhancement of the speed of the impinging flow due to deflection away from a mountain range to the south of the area of extreme precipitation. Both these effects are important for better forecasting during similar synoptic situations in the future. Finally, an accurate prediction of the winds in Central Norway may be dependent on the representation of a baroclinic system to the southeast of Newfoundland 3 d earlier.

7. Acknowledgments

References

Andersson, A., Bakan, S., Fennig, K., Grassl, H., Klepp, C. H. and co-authors. 2007. Hamburg Ocean Atmosphere Parameters and Fluxes from Satellite Data - HOAPS-3: twice daily composite. *World Data Center for Climate* doi: 10.1594/WDCC/HOAPS3_DAILY

Beldring, S., Engen-Skaugen, T., Førland, E. J. and Roald, L. A. 2008. Climate change impacts on hydrological processes in Norway based on two methods for transferring regional climate model results to meteorological station sites. *Tellus* **60A**, 439–450.

Benestad, R. E. and Haugen, J. E. 2007. On complex extremes: flood hazards and combined high spring-time precipitation and temperature in Norway. *Clim. Change* **85**, 381–406. doi:10.1007/s10584-007-9263-2.

Draxler, R. R. and Rolph, G. D. 2010. HYSPLIT (HYbrid Single-Particle Lagrangian Integrated Trajectory) Model access via NOAA ARL READY Website (http://ready.arl.noaa.gov/HYSPLIT.php). NOAA Air Resources Laboratory, Silver Spring, MD, U.S.A.

Hagen, B. 2008. *Wind extremes in the Nordic Seas: dynamics and forecasting*, Master Thesis, Geophysical Institute, University of Bergen

Hanssen-Bauer, I., Førland, E. J., Haugen, J. E. and Tveito, O. E. 2003. Temperature and precipitation scenarios for Norway: comparison of results from dynamical and empirical downscaling.. *Clim. Res.* **25**, 15–27.

Haugen, J. E. and Iversen, T. 2008. Response in extremes of daily precipitation and wind from a downscaled multi-model ensemble of anthropogenic global climate change scenarios.. *Tellus* **60A**, 411–426.

Holton, J. R. 2004. *An Introduction to Dynamic Meteorology.* 4th Edition, Elsevier Academic press, London, 164 pp.

Hunt, J. C. R., Ólafsson, H. and Bougeault, P. 2001. Coriolis effects on orographic and mesoscale flows. *Q. J. R. Meteorol. Soc.* **56**, 601–633.

Kalnay, E. and co-authors. 1996. The NCEP/NCAR Reanalysis 40-year Project. *Bull. Am. Meteorol. Soc.* **77**, 437–471.

Mohr, M. 2008. New routines for gridding of temperature and precipitation observations for 'seNorge.no'.. Met.no Report, pp. 40.

Ólafsson, H. and Bougeault, P. 1996. Nonlinear flow past an elliptic mounatin ridge. *J. Atmos. Sci.* **127**, 2465–2489.

Ólafsson, H. and Bougeault, P. 1997. The effect of rotation and surface friction on orographic drag. *J. Atmos. Sci.* **54**, 193–210.

Ólafsson, H. 2000. The impact of flow regimes on asymmetry of orographic drag at moderate and low Rossby numbers. *Tellus* **52A**, 365–379.

Pierrehumbert, R. T. and Wyman B. 1985. Upstream effects of mesoscale mountains. *J. Atmos. Sci.* **42**, 977–1003.

Rabier, F., Klinker, E., Courtier, P. and Hollingsworth, A. 1996. Sensitivity of forecast errors to initial conditions. *Q. J. R. Meteorol. Soc.* **122**, 121–150.

Reuder, J., Fagerlid, G. O., Barstad, I. and Sandvik, A. 2007. Stord Orographic Precipitation Experiment (STOPEX): an overview of phase 1.. *Adv. Geosci.* **10**, 17–23.

Rolph, G. D. 2010. Real-time Environmental Applications and Display System (READY) Website (http://ready.arl.noaa.gov). NOAA Air Resources Laboratory, Silver Spring, MD, U.S.A.

Skamarock, W. C., Klemp, J. B., Dudhia, J., Gill, D. O., Barker, D. M. and co-authors. 2008. A Description of the Advanced Research WRF Version 3.. Ncar technical Note, p. 125.

Stohl, A., Forster, C. and Sodemann, H. 2008. Remote sources of water vapor forming precipitation on the Norwegian west coast at 60 N°: a tale of hurricanes and an atmospheric river. *J. Geophys. Res.-Atmos.* **D113**, 402–416.

Tveita, B. 2008. *Extreme winds in the Nordic Seas: an observational and numerical study*, Master thesis, Geophysical Institute, University of Bergen.

Wentz, F. J. and Spencer, R. W. 2008. SSM/I Rain Within an Unified All-Weather Ocean Algoritm. *J. Atmos. Sci.* **55**, 1613–1627.